Store-operated Ca2+ entry modulates sarcoplasmic reticulum Ca2+ loading in neonatal rabbit cardiac ventricular myocytes

Jingbo Huang, Casey van Breemen, Kuo-Hsing Kuo, Leif Hove-Madsen and Glen F. Tibbits

Am J Physiol Cell Physiol 290:1572-1582, 2006. First published Jan 18, 2006;
doi:10.1152/ajpcell.00226.2005

AJP - Cell Physiology is dedicated to innovative approaches to the study of cell and molecular physiology. It is published 12 times a year (monthly) by the American Physiological Society, 9650 Rockville Pike, Bethesda MD 20814-3991. ISSN: 0363-6143, ESSN: 1522-1563. Visit our website at http://www.the-aps.org/.

Am J Physiol Cell Physiol 290: C1572–C1582, 2006.
First published January 18, 2006; doi:10.1152/ajpcell.00226.2005.

Store-operated Ca^{2+} entry modulates sarcoplasmic reticulum Ca^{2+} loading in neonatal rabbit cardiac ventricular myocytes

Jingbo Huang,[1,2] Casey van Breemen,[2,3] Kuo-Hsing Kuo,[3] Leif Hove-Madsen,[4] and Glen F. Tibbits[1,2]

[1]*Cardiac Membrane Research Laboratory, Simon Fraser University, Burnaby;* [2]*Cardiovascular Sciences, Child and Family Research Institute, Vancouver;* [3]*Department of Anesthesiology, Pharmacology and Therapeutics, University of British Columbia, Vancouver, British Columbia, Canada; and* [4]*Laboratorio de Fisiología Celular, Cardiología, Hospital de Sant Pau, Barcelona, Spain*

Submitted 11 May 2005; accepted in final form 5 January 2006

Huang, Jingbo, Casey van Breemen, Kuo-Hsing Kuo, Leif Hove-Madsen, and Glen F. Tibbits. Store-operated Ca^{2+} entry modulates sarcoplasmic reticulum Ca^{2+} loading in neonatal rabbit cardiac ventricular myocytes. *Am J Physiol Cell Physiol* 290: C1572–C1582, 2006. First published January 18, 2006; doi:10.1152/ajpcell.00226.2005.—Store-operated Ca^{2+} entry (SOCE), which is Ca^{2+} entry triggered by the depletion of intracellular Ca^{2+} stores, has been observed in many cell types, but only recently has it been suggested to occur in cardiomyocytes. In the present study, we have demonstrated SOCE-dependent sarcoplasmic reticulum (SR) Ca^{2+} loading ($load_{SR}$) that was not altered by inhibition of L-type Ca^{2+} channels, reverse mode Na^+/Ca^{2+} exchange (NCX), or nonselective cation channels. In contrast, lowering the extracellular [Ca^{2+}] to 0 mM or adding either 0.5 mM Zn^{2+} or the putative store-operated channel (SOC) inhibitor SKF-96365 (100 μM) inhibited $load_{SR}$ at rest. Interestingly, inhibition of forward mode NCX with 30 μM KB-R7943 stimulated SOCE significantly and resulted in enhanced $load_{SR}$. In addition, manipulation of the extracellular and intracellular Na^+ concentrations further demonstrated the modulatory role of NCX in SOCE-mediated SR Ca^{2+} loading. Although there is little knowledge of SOCE in cardiomyocytes, the present results suggest that this mechanism, together with NCX, may play an important role in SR Ca^{2+} homeostasis. The data reported herein also imply the presence of microdomains unique to the neonatal cardiomyocyte. These findings may be of particular importance during open heart surgery in neonates, in which uncontrolled SOCE could lead to SR Ca^{2+} overload and arrhythmogenesis.

cardiac ontogeny; cardiac excitation-contraction coupling; calcium homeostasis

IT IS WELL DOCUMENTED that the depletion of intracellular Ca^{2+} stores (sarcoplasmic reticulum/endoplasmic reticulum, SR/ER) triggers Ca^{2+} entry (store-operated Ca^{2+} entry, SOCE) in many nonexcitable cells, vascular smooth muscle cells (7, 8, 30), and skeletal muscle cells (22, 23). The mechanisms for linking intracellular stores to the plasma membrane are not well understood (33). One hypothesis proposed by Putney (31) that has gained some acceptance is that intracellular Ca^{2+} stores are linked by the release of a Ca^{2+} influx factor (CIF). After the depletion of Ca^{2+} stores, CIF is postulated to diffuse to the plasma membrane and activate the store-operated channels (SOCs). Fasolato et al. (10) suggested the exocytosis model, in which channels may be inserted into the membrane by vesicle fusion in response to Ca^{2+} store depletion. Another hypothesis put forth is that Ca^{2+} regulation or the depletion of stores might result in a fall in $[Ca^{2+}]_i$ in a restricted space between the plasma membrane and closely associated ER, which in turn activates the channels (3). At present, the favored model for SOCE is the conformational coupling model, in which the discharge of Ca^{2+} stores causes a conformational change that triggers direct protein-protein interaction between Ca^{2+} stores and the SOCs. It is distinctly possible that there are different mechanisms for SOCE in different cell types. It has been demonstrated that SOCE plays an important role in a variety of physiological functions, such as contraction, secretion, cell growth, and proliferation in different cell types. However, until its recent demonstration in murine cardiomyocytes (19, 20, 37), it had generally been accepted that SOCE does not exist in cardiomyocytes. The present study was based on our observation that the SR in neonatal myocytes was refilled with Ca^{2+} within 10 s after caffeine (CAF)-induced depletion of SR Ca^{2+} while voltage clamped at −80 mV. Our results reported herein demonstrate the robust presence of SOCE in neonatal rabbit ventricle myocytes, which decreases significantly with ontogeny.

MATERIALS AND METHODS

Isolation of ventricular myocytes. Ventricular myocytes were isolated from the hearts of New Zealand White rabbits of either sex from three distinct age groups, 3 days (3d), 10 days (10d), and 56 days (56d) postpartum, using methods described previously (17, 34). In the 56d group, 25 mg of Yakult collagenase in 150 ml of a nominally Ca^{2+}-free solution, 5 mg of protease in 50 ml of storage solution, and a pump speed of 4 ml/min were used. The experiments described in this study were approved by the University Animal Care Committee at Simon Fraser University (permit no. 698K-96) and conformed to the guidelines established by the Canadian Council on Animal Care.

Whole cell perforated patch-clamp voltage. A whole cell amphotericin-perforated voltage-clamp technique was used at room temperature as described previously (17). The internal pipette solution contained (in mM) 110 CsCl, 5 MgATP, 1 $MgCl_2$, 20 tetraethylammonium (TEA), 5 Na_2 phosphocreatine, and 10 HEPES at pH 7.1 adjusted with CsOH. The standard external solution contained (in mM) 130 NaCl, 5 CsCl, 1 $MgCl_2$, 2.0 $CaCl_2$, 5 Na^+-pyruvate, 10 glucose, and 10 HEPES at pH 7.4 adjusted with NaOH. In some experiments, the cells were perfused with a nominally Ca^{2+}-free solution (referred to herein as 0 mM) or with different internal and external Na^+ concentrations ($[Na^+]_i$ and $[Na^+]_o$, respectively, and 125 and 14 mM, respectively, with the difference from standard external solution being replaced with CsCl). Only cells in which the access resistance was <20 MΩ were used in these experiments.

Address for reprint requests and other correspondence: G. F. Tibbits, Cardiac Membrane Research Laboratory, Simon Fraser Univ., 8888 University Dr., Burnaby, BC, Canada V5A 1S6 (e-mail: tibbits@sfu.ca).

The costs of publication of this article were defrayed in part by the payment of page charges. The article must therefore be hereby marked "*advertisement*" in accordance with 18 U.S.C. Section 1734 solely to indicate this fact.

Measurement of Ca^{2+} fluorescence. Cytosolic Ca^{2+} concentration ($[Ca^{2+}]_i$) was measured using the fluorescent Ca^{2+} indicator fluo-3 AM as described previously (17). F_0 was assumed to be the difference between background fluorescence determined in the absence and presence of a cell in the area of measurement. ΔF is the increment measured from baseline or the background fluorescence in the presence of a cell-free area. F_{max} was the fluorescence acquired after the cell was depolarized to +200 mV for 10–20 s to flood the cytosol with Ca^{2+} at the end of each experiment.

Electron microscopy. Images of the cross sections of the ventricular muscle myocytes were obtained with a Phillips 300 electron microscope as described previously (13). Briefly, each heart was perfused for 15 min using a Langendorff apparatus at age-appropriate perfusion speeds (37°C). After initial fixation, the hearts were removed from the Langendorff apparatus. The ventricle was trimmed into small blocks of ~0.5 × 0.5 × 0.5 mm and immersed in the fixative for 2 h at 4°C on a shaker. The blocks were then washed three times in 0.1 M sodium cacodylate (10 min each). In the process of secondary fixation, the blocks were placed into 1% OsO_4-0.1 M sodium cacodylate buffer for 2 h and then were washed three times with distilled water (10 min each). The blocks were then treated with 1% uranyl acetate for 1 h (en bloc staining), followed by being washed with distilled water. Increasing concentrations of ethanol (50%, 70%, 80%, 90%, and 95%) were used (10 min each) in the process of dehydration. Ethanol (100%) and propylene oxide were used (three 10-min washes each) for the final process of dehydration. The blocks were infiltrated overnight in the resin (TAAB 812) and then embedded in molds and polymerized in an oven at 60°C for 8–10 h. The embedded blocks were sectioned on a microtome using a diamond knife and placed on 400-mesh copper grids. The section thickness was ~80 nm. The sections were then stained with 1% uranyl acetate (4 min) and Reynolds lead citrate (3 min) and imaged using a Phillips 300 electron microscope. Twenty-five sections from each of three hearts for each of two age groups (3d and 56d) were used for statistical analysis.

Data analysis. Data are means ± SE. The statistical significance of the results was tested using one-way ANOVA with SPSS version 11.0 software (SPSS, Chicago, IL) or Student's *t*-test for paired or unpaired samples. Post hoc tests were performed using Tukey's multiple-comparison test. $P \leq 0.05$ was considered statistically significant.

RESULTS

SR Ca^{2+} loading after clearance of SR Ca^{2+} content was prominent in newborns and diminished with age. To determine whether there was significant SOCE-dependent sarcoplasmic reticulum (SR) Ca^{2+} loading ($load_{SR}$) after clearance of the SR Ca^{2+} content, the protocol shown in Fig. 1*A* was used. The first rapid 10 mM CAF application was used to clear the Ca^{2+} stored in the SR before the protocol indicated. The integrals of Na^+/Ca^{2+} exchanger current (I_{NCX}) elicited by the second and third CAF applications were used to determine the $load_{SR}$ during the preceding 10- and 60-s intervals. During the entire experiment, the cell was voltage clamped at −80 mV (resting condition). The duration of CAF application was limited to 8 s to prevent a possible increase in intracellular cAMP concentration that could potentially result from longer exposure times (36) and confound the results. Figure 1*B* shows representative traces of membrane current and $[Ca^{2+}]_i$ in 3d, 10d, and 56d myocytes superfused with control solution (CON). There was measurable $load_{SR}$ after clearance of SR Ca^{2+} content in the 3d and 10d myocytes and substantially less $load_{SR}$ in 56d cells. $Load_{SR}$ was significantly enhanced when the perfusion time was increased from 10 to 60 s as shown in Fig. 1*C*. There were significant decreases in $load_{SR}$ with age with regard to both the 10- and 60-s intervals.

$Load_{SR}$ at rest depends on sarcolemmal Ca^{2+} entry but not on I_{Ca} or reverse mode NCX. To investigate whether the prominent $load_{SR}$ at rest was due to Ca^{2+} entry through Ca^{2+} current (I_{Ca}) or reverse mode NCX, $load_{SR}$ during the 60-s interval was determined in the presence of 10 μM nifedipine (NIF), an L-type Ca^{2+} channel blocker, and 5 μM KB-R 7943 (KB-R), a blocker primarily of reverse mode NCX and to a lesser degree of I_{Ca}, as shown in Fig. 2*A*. Figure 2*A*, *top*, shows the sequence of events during the experimental protocol. With this design, the integrals of the second and third CAF-induced I_{NCX} (shown in gray) reflected the $load_{SR}$ in the 60-s interval in CON and in NIF + KB-R solutions, respectively. There were no reductions in $load_{SR}$ with NIF + KB-R for both 3d and 56d myocytes compared with CON solution. Furthermore, there were no appreciable changes in the fluorescence baseline ($\Delta F/F_0$) during 60-s $load_{SR}$ (data not shown).

To determine whether $load_{SR}$ at rest was due to another source of sarcolemmal Ca^{2+} entry, the effect of removal of extracellular $[Ca^{2+}]$ ($[Ca^{2+}]_o$) on $load_{SR}$ was examined in 3d cells in which $load_{SR}$ was significantly more robust. Figure 2*B* shows three representative membrane current traces induced by CAF application after a 10-s loading period, with either 2.0 or 0 mM $[Ca^{2+}]_o$ in a 3d myocyte. External Mg^{2+} concentration ($[Mg^{2+}]_o$) was increased to 3 mM in the 0 mM $[Ca^{2+}]_o$ solution to improve seal stability. As shown in Fig. 2, CAF-induced I_{NCX} was abolished by perfusion with 0 mM $[Ca^{2+}]_o$ and was restored after reperfusion with 2 mM $[Ca^{2+}]_o$.

Increased $[Ca^{2+}]_i$ as consequence of SOCE. The results shown in Figs. 1 and 2 suggest that $load_{SR}$ at rest occurs through SOCE or nonselective cation channels (NSCCs). To test this hypothesis, a classical approach based on readdition of 2 mM $[Ca^{2+}]_o$ after transient extracellular Ca^{2+} removal (32) was used to evaluate the role of SOCE. Figure 3, *A* and *B*, shows representative Ca^{2+} transient traces measured during fast switching from 0 to 2 mM $[Ca^{2+}]_o$ for 3d and 56d myocytes, respectively. These data were collected in the presence of 10 μM NIF and 5 μM KB-R, both with and without SR Ca^{2+} depletion. SR Ca^{2+} depletion was achieved by continuous stimulation of the cell with depolarization (from −80 mV to +10 mV for 400 ms every 5 s) in the presence of 25 μM cyclopiazonic acid (CPA), a blocker of the SR Ca^{2+} pump, and 10 μM ryanodine (Ry), which locks the Ry receptor (RyR) in a subconducting open state. CAF (10 mM) was applied rapidly to verify that SR Ca^{2+} depletion was complete (see Supplemental Fig. 1; http://ajpcell.physiology.org/cgi/content/full/00226.2005/DC1). SOCE was then induced by a 10-s perfusion of 0 mM $[Ca^{2+}]_o$ solution, followed by readdition of 2 mM $[Ca^{2+}]$. This caused a substantial increase in $[Ca^{2+}]_i$ in the 3d myocyte (Fig. 3*A*) but a significantly smaller increase in the 56d myocyte (Fig. 3*B*). $[Ca^{2+}]_i$ reached a steady state within ~100 s of switching solutions. It is important to note that an increase in $[Ca^{2+}]_i$ was not observed when the SR was fully loaded with Ca^{2+}, which is clearly shown in Fig. 3, *A–C*.

Pharmacological inhibition of $load_{SR}$ and SOCE. Because little evidence of SOCE was observed in the 56d group, the effects of different blockers on $load_{SR}$ and SOCE were investigated in 3d myocytes only, using a 60-s SR loading interval as described in Fig. 1*A*. We investigated 30 μM KB-R, a blocker of both reverse mode and forward mode NCX at this concentration (1); 50–200 μM SKF-96365 (SKF) and 50–150 μM 2-aminoethoxydiphenyl borate (2-APB), both putative block-

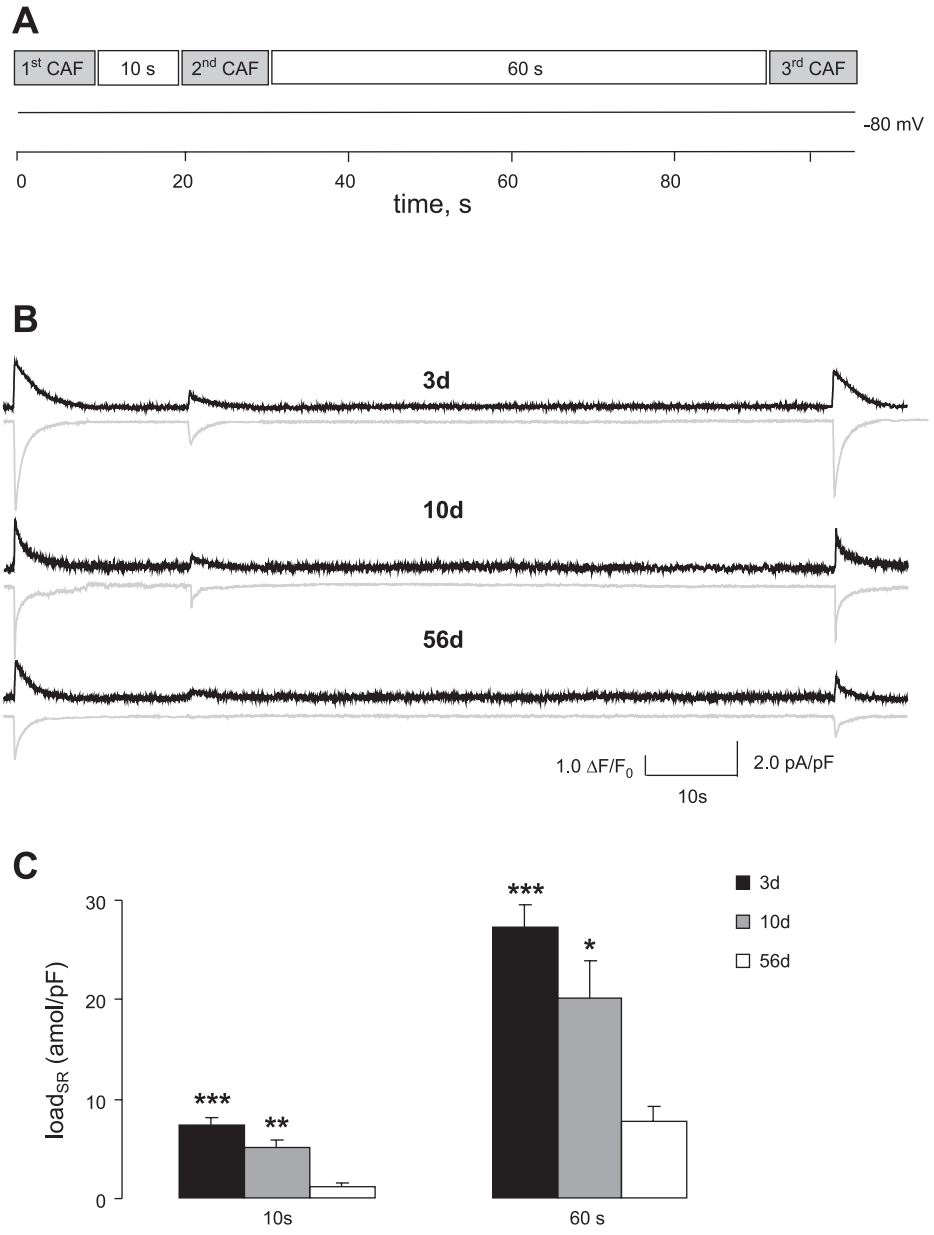

Fig. 1. Time and age dependence of store-operated Ca^{2+} entry (SOCE)-dependent sarcoplasmic reticulum (SR) Ca^{2+} loading ($load_{SR}$) under resting conditions. *A*: protocol used to measure $load_{SR}$ during 10- and 60-s intervals. The integrals of Na^+/Ca^{2+} exchanger current (I_{NCX}) induced by second and third caffeine (CAF) applications were used to determine the amount of $load_{SR}$. *B*: 3 representative traces measured using the protocol described in *A* in ventricular myocytes isolated from hearts of New Zealand White rabbits of either sex from three distinct age groups: 3 days (3d), 10 days (10d), and 56 days (56d) postpartum. Ca^{2+} transients are traced in black, and membrane potentials (E_m) are traced in gray. *C*: bar graphs of $load_{SR}$ after 10- and 60-s intervals in 3d (solid bars), 10d (gray bars), and 56d (open bars). There were significant differences in $load_{SR}$ (normalized by E_m) between 3d and 56d myocytes (***$P < 0.0001$ for 10- and 60-s loading) and between 10d and 56d myocytes (**$P < 0.005$ for 10 s and *$P < 0.05$ for 60-s loading). There were also significant differences between 10- and 60-s loading for each age group. $n = 15$; $P < 0.0001$.

ers of SOCE (25, 26); 30–100 μM (*R*,*S*)-(3,4-dihydro-6,7-dimethoxy-isoquinoline-1-yl)-2-phenyl-*N*,*N*-di[2-(2,3,4-trimethoxyphenyl)ethyl]acetamide (LOE-908), a blocker of NSCC (21); and 0.5 mM $ZnCl_2$, a competitive cation inhibitor. It should be noted, however, that 30 μM KB-R is a relatively high dose of this lipophilic drug, and one must consider possible nonspecific effects in the interpretation of these results. As shown in Fig. 4, $load_{SR}$ decreased significantly in the presence of 100 μM SKF and 0.5 mM $ZnCl_2$. However, up to 100 μM LOE-908 and up to 150 μM 2-APB did not change $load_{SR}$ significantly. Surprisingly, 30 μM KB-R significantly increased $load_{SR}$ under these conditions. Application of 10 μM nifedipine did not have a significant effect on $load_{SR}$ (data not shown).

To corroborate the results shown in Fig. 4, the effects of the different blockers were also tested using the method described in Fig. 3. As shown in Fig. 5*A*, the increase in $[Ca^{2+}]_i$ was significantly inhibited in the presence of SKF. Figure 5*B* shows that there was a substantial rise in $[Ca^{2+}]_i$ that eventually reached the steady state after $[Ca^{2+}]_o$ was switched from 0 to 2 mM while the cell was voltage clamped at −80 mV. $[Ca^{2+}]_i$ increased further after the application of 30 μM KB-R, and hyperpolarizing the membrane potential (E_m) from −80 to −120 mV caused an additional rise in $[Ca^{2+}]_i$. However, the rate of $[Ca^{2+}]_i$ rise with 30 μM KB-R (at −80 mV or −120 mV) was slower than that observed under control conditions because of higher $[Ca^{2+}]_i$. Figure 5*C* shows the steady-state $[Ca^{2+}]_i$ (expressed as $\Delta F/F_0$) after $[Ca^{2+}]_o$ was switched from 0 to 2 mM in control solution, 30 μM KB-R, or 100 μM SKF. The magnitude of the rise in $[Ca^{2+}]_i$ in the presence of KB-R and SKF was significantly different from that observed under control conditions. Neither LOE-908 nor 2-APB had a significant effect on $[Ca^{2+}]_i$ compared with the control group (data not shown).

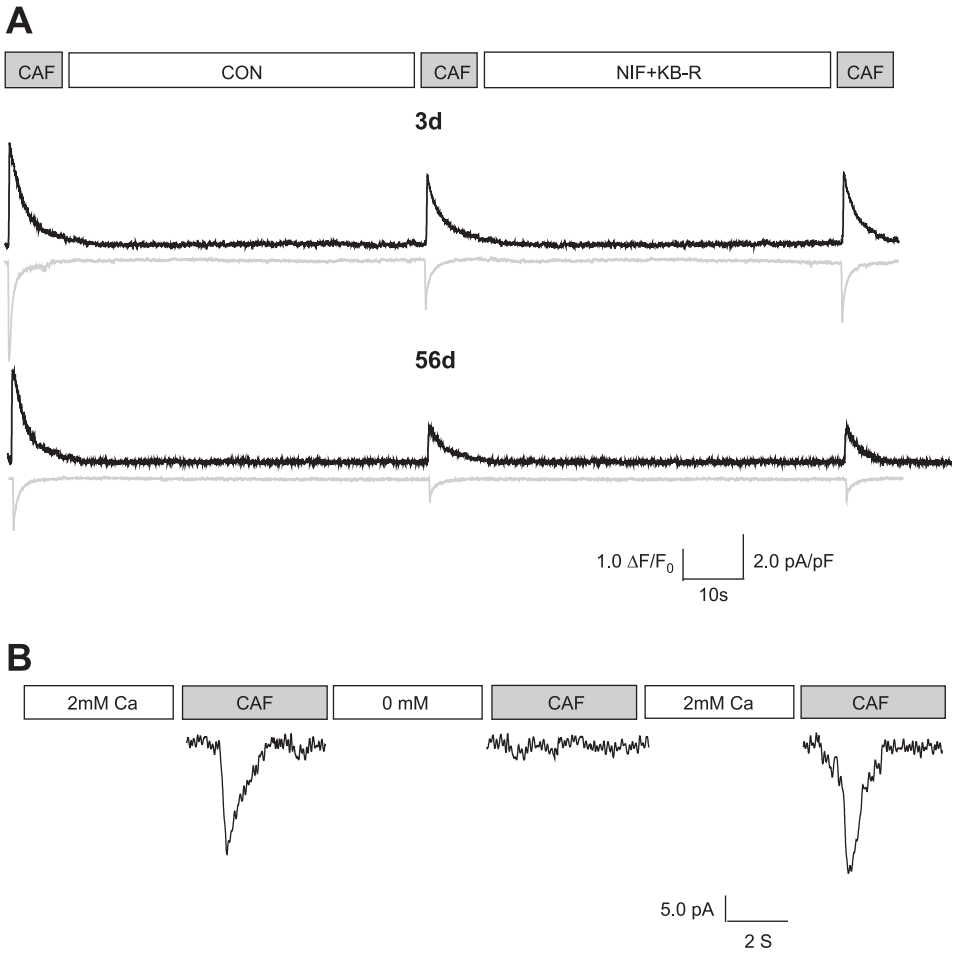

Fig. 2. $Load_{SR}$ is dependent on extracellular Ca^{2+} concentration ($[Ca^{2+}]_o$) but is not the result of SOCE through L-type Ca^{2+} current (I_{Ca}) and/or reverse mode I_{NCX}. *A*: representative membrane current (gray trace) and Ca^{2+} transient (black trace) of 60-s interval loading in presence of control (CON) and 10 μM nifedipine (NIF) + 5 μM KB-R7943 (KB-R) (NIF + KB-R) solutions in sequence. The first CAF-induced I_{NCX} was used to clear sarcoplasmic reticulum (SR) Ca^{2+} content. The integrals of the second and third CAF-induced I_{NCX} were used to evaluate $load_{SR}$ in CON and NIF + KB-R, respectively, during 60-s interval. *B*: 3 representative E_m traces induced by CAF application after 10-s loading intervals with 2 mM (*left*), 0 mM (*middle*), and 2 mM $[Ca^{2+}]_o$ (*right*) in a 3d myocyte.

Modulation of $load_{SR}$ by NCX activity. To investigate further the modulation of $load_{SR}$ by NCX, $load_{SR}$ during 10- and 60-s intervals was investigated with different $[Na^+]_o$ and $[Na^+]_i$. Three different groups of $[Na^+]_o$ and $[Na^+]_i$ combinations were used: 140/10, 125/10, and 125/14 mM, respectively, for $[Na^+]_o/[Na^+]_i$. As shown in Fig. 6*A*, there were significant differences in $load_{SR}$ measured on the basis of the CAF-induced I_{NCX} integral for the 10-s interval between 125/14 vs. 125/10 mM and 140/10 mM concentration combinations and for the 60-s interval between 140/10 vs. 125/14 mM concentration combinations. As shown in Fig. 6*B*, $load_{SR}$ during the 10-s interval was significantly increased in the presence of 30 μM KB-R for both the 125/10 and 140/10 concentration combination groups. The magnitude of increase was significantly greater in the 140/10 group compared with the 125/10 group.

Voltage dependence of $load_{SR}$. Because the driving forces for reverse mode NCX- and SOCE-mediated $load_{SR}$ have opposite voltage dependencies, $load_{SR}$ was examined in 3d myocytes as a function of E_m (Fig. 7*C*). E_m was switched from −80 mV to −50 mV, −80 mV, −110 mV, or −140 mV for 10 s. CAF application before each depolarization was used to clear SR Ca^{2+}, and the I_{NCX} integral induced by the second CAF application was used to determine $load_{SR}$ at the four different E_m values. Figure 7*B* shows representative CAF-induced I_{NCX} at the indicated loading voltages in CON and with 10 μM NIF plus 30 μM KB-R (NIF + KB-R). For the test potentials −140 mV, −110 mV, and −80 mV, $load_{SR}$ was significantly greater in the presence of NIF + KB-R (Fig. 7*C*). $Load_{SR}$ in the control group showed a parabolic increase with E_m held at less negative potentials. With NIF + KB-R, however, there was an inverse relationship between $load_{SR}$ and E_m that was well fitted ($R^2 = 0.98$) using linear regression analysis.

Subsarcolemma cisternal structure during development. Figure 8*A* shows representative cross-sectional electron photomicrographs of 3d and 56d myocytes. For clarification, ×1.67 magnification of the subsarcolemma cisternal (SSC) structure is shown (Fig. 8*A*, *insets*). The cleft between the sarcolemma (SL) and the SSC was ~20 nm for both 3d and 56d myocytes. The SSC in the 56d myocytes form a tubulelike appearance as documented previously for a variety of adult mammalian species. The SSC in the 3d myocytes appeared to form sheetlike structures that extended along the apposing SL and were determined to be, on average, about three times longer than those in the 56d myocytes.

DISCUSSION

$Load_{SR}$ under resting conditions as a consequence of SL Ca^{2+} entry. The observation that the SR loaded with Ca^{2+} during the 10- and 60-s intervals after CAF-induced SR Ca^{2+} depletion while the cell was voltage clamped at −80 mV (Fig. 1) is difficult to explain on the basis of present knowledge of

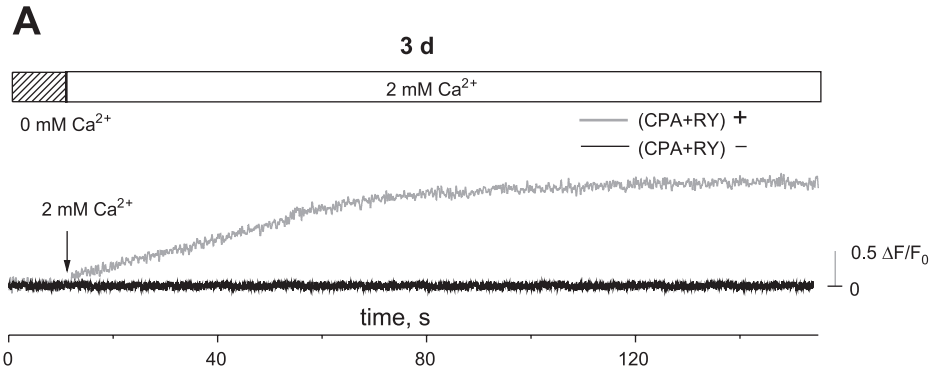

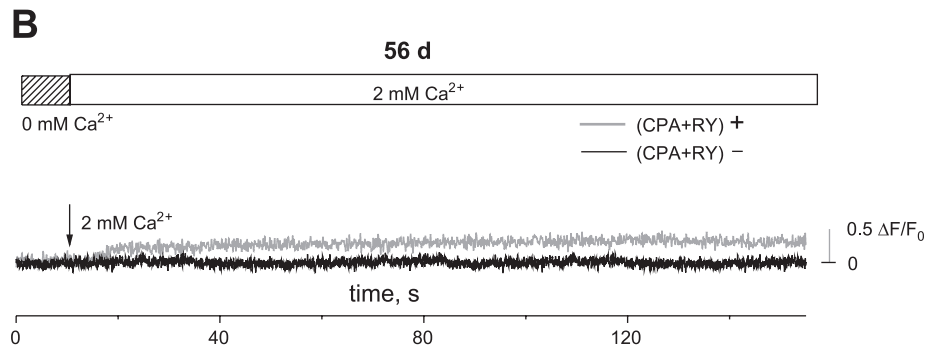

Fig. 3. Intracellular $[Ca^{2+}]$ ($[Ca^{2+}]_i$) increase as a consequence of SOCE in cardiac myocytes. *A* and *B*: representative Ca^{2+} transient traces measured with both depleted SR Ca^{2+} [cyclopiazonic acid (CPA) + ryanodine $(Ry)^+$, gray trace] and fully loaded SR Ca^{2+} [$(CPA + Ry)^-$, black trace]. *A*: 3d myocyte preperfused with and without CPA + Ry as well as with 10 μM NIF + 5 μM KB-R. $[Ca^{2+}]_o$ was switched from 0 mM (for 10 s) to 2 mM (arrow). *B*: response of $[Ca^{2+}]_i$ in a 56d myocyte to conditions shown in *A*. *C*: magnitude of $[Ca^{2+}]_i$ rise after $[Ca^{2+}]_o$ was switched from 0 to 2 mM in both $(CPA + Ry)^+$ and $(CPA + Ry)^-$ in 3d (solid bar), 10d (gray bar), and 56d (open bar), respectively. $[Ca^{2+}]_i$ was significant greater in 3d than in 56d myocytes (***$P < 0.0001$) and in 10d than in 56d myocytes (*$P < 0.05$) in the presence of CPA and Ry. An increase of $[Ca^{2+}]_i$ was not observed in the absence of CPA and Ry. $n = 6$.

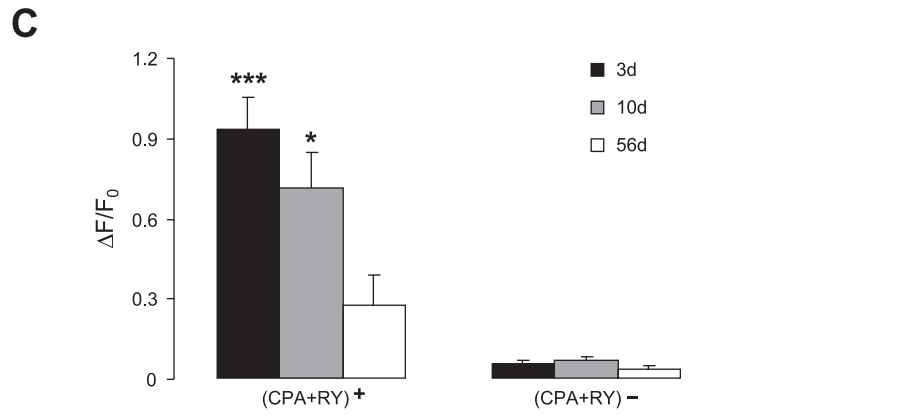

the mechanisms of transsarcolemmal Ca^{2+} influx in cardiomyocytes, because one assumes that voltage-gated Ca^{2+} channels are not activated and reverse mode NCX activity is not favored under these conditions (see Supplemental Table 1). These assumptions were supported by the lack of a detectable membrane current during these loading periods. The Ca^{2+} source for $load_{SR}$ could be from organelles or from the extracellular space. In this study, we present strong evidence that the $load_{SR}$ was due to Ca^{2+} entry from external Ca^{2+} as demonstrated by the $[Ca^{2+}]_o$ dependence of $load_{SR}$ (Fig. 2*B*). Furthermore, because the $load_{SR}$ was observed at −80 mV and was resistant to 5 μM KB-R and 10 μM NIF (Fig. 2*A*), Ca^{2+} entry is unlikely to have occurred through reverse mode NCX or I_{Ca}.

SOCE in cardiac myocytes. The notion that the depletion of SR or ER could initiate the activation of plasma membrane Ca^{2+} entry through SOCs was first proposed in smooth muscles more than two decades ago, and the time of activation has

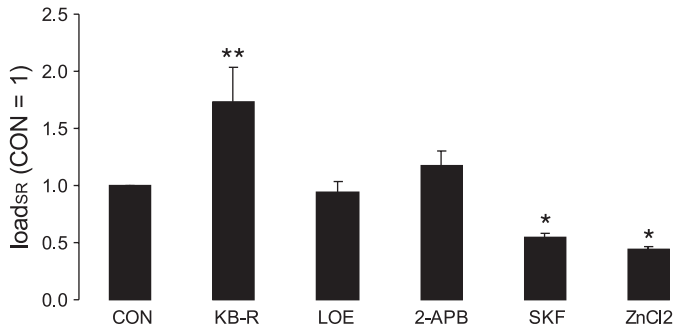

Fig. 4. Effect of blockers on $load_{SR}$ in 3d myocytes. Effects of blockers on 60-s $load_{SR}$ were normalized to that of CON (taken as unity). $Load_{SR}$ significantly increased in the presence of 30 μM KB-R (**$P < 0.01$) and decreased in the presence of either 100 μM SKF-96365 (SKF) or 0.5 mM $ZnCl_2$ (*$P < 0.05$ for both). 100 μM (*R*,*S*)-(3,4-dihydro-6,7-dimethoxy-isoquinoline-1-yl)-2-phenyl-*N*,*N*-di[2-(2,3,4-trimethoxyphenyl)ethyl]acetamide (LOE-908), a blocker of nonselective cation channels (NSCCs), and 150 μM 2-aminoethoxydiphenyl borate (2-APB) did not show any significant effect on $load_{SR}$. $n = 10$.

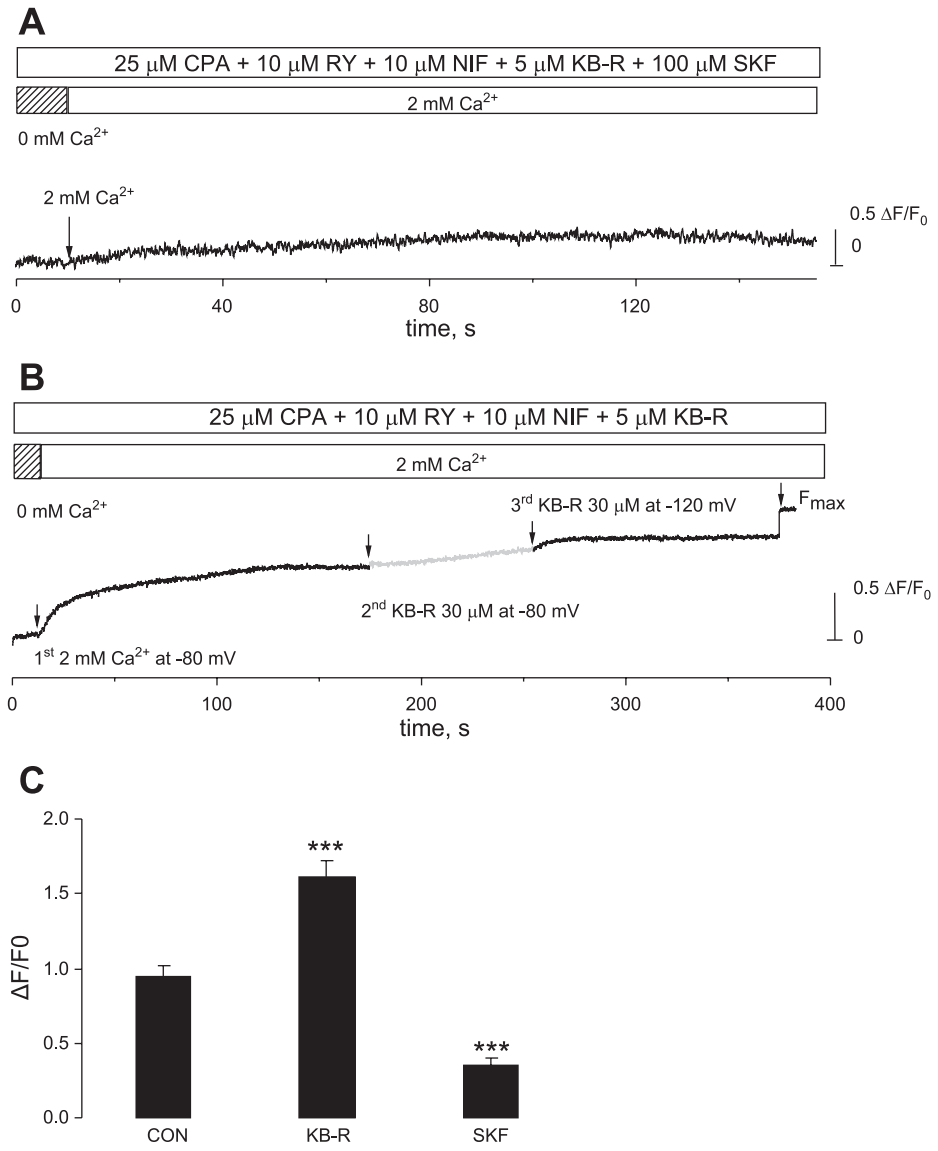

Fig. 5. Effect of blockers on SOCE in 3d myocytes. *A* and *B*: representative Ca^{2+} transient traces measured in response to switching $[Ca^{2+}]_o$ from 0 to 2 mM in the presence of 10 μM NIF and 5 μM KB-R after clearance of SR Ca^{2+} as described in Fig. 3. *A*: trace from a cell voltage clamped at −80 mV and pretreated and perfused with 100 μM SKF. *B*: holding potential of −80 mV (black trace at *left*) followed by application of 30 μM KB-R (gray trace) and hyperpolarization to −120 mV (black trace at *right*). *C*: effect of blockers on Ca^{2+} transient rise ($\Delta F/F_0$) induced by switching $[Ca^{2+}]_o$ from 0 to 2 mM after depletion of SR Ca^{2+}. Magnitude of rise in $[Ca^{2+}]_i$ in the presence of KB-R and SKF was significantly different from that observed under control conditions. $n = 8$; $^{***}P < 0.001$.

been investigated in a variety of nonexcitable (7) and excitable cells, including smooth muscle (7, 8, 30, 42) and skeletal muscle cells (23). Another type of plasma membrane Ca^{2+} entry appears to be selective predominantly for Na^+ over Ca^{2+} via the NSCC. Ca^{2+} influx through most SOCs can be blocked by the divalent cations Zn^{2+}, Cd^{2+}, Mn^{2+}, Ni^{2+}, and Ba^{2+} and by the trivalent cations La^{3+} and Gd^{3+} (2). Although it could be argued that Zn^{2+} may have some effect on Na^+ and K^+ channels, the presence of Zn^{2+} under our experimental conditions (−80 mV and K^+ replacement) is unlikely to introduce any confounding consequences. Unfortunately, the lack of highly specific pharmacological tools has considerably impaired the identification of SOCs. SKF and 2-APB have been demonstrated as putative blockers of SOCE. LOE-908 has been implicated as an inhibitor of Ca^{2+}-permeable NSCCs, but it did not inhibit SOCE in our present experiments.

In the current study, the two basic experimental protocols based on SR Ca^{2+} reloading after CAF exposure and readdition of Ca^{2+} after exposure to Ca^{2+}-free extracellular solution both provided strong support for a robust SOCE in resting neonatal cardiac myocytes. Furthermore, significant inhibition of $load_{SR}$ during the 60-s interval by both Zn^{2+} and SKF (Fig. 4), as well as the significant reduction of $[Ca^{2+}]_i$ caused by SKF (Fig. 5*A*) but insensitivity to LOE-908, provides strong support for SOCE rather than nonspecific Ca^{2+} entry.

The interpretation of the effects of 2-APB is more complex. It has been known for some time that 2-APB is an inhibitor of inositol 1,4,5-trisphosphate (IP_3) receptors (IP_3Rs) (25) and at doses of 50–100 μM, 2-APB has been exploited to examine the role of IP_3-mediated SOCE. However, 2-APB within the same concentration range also has been reported to inhibit a variety of transient receptor potential (TRP) channels, including subclasses of TRP melastatin (TRPM) channels and TRP vanilloid-related (TRPV) channels, some of which are purported to be responsible for SOCE (5, 6, 20, 37). Furthermore, higher doses of 2-APB increased Ca^{2+} influx in rat basophilic leukemia (RBL)-2H3 mast cells (≥100 μM) (6) and heterologously expressed TRPV1–TRPV3 channels (>200 μM) (16). In the present study, we found that there were no significant differences in $load_{SR}$ between 0, 50, 75, and 150 μM 2-APB

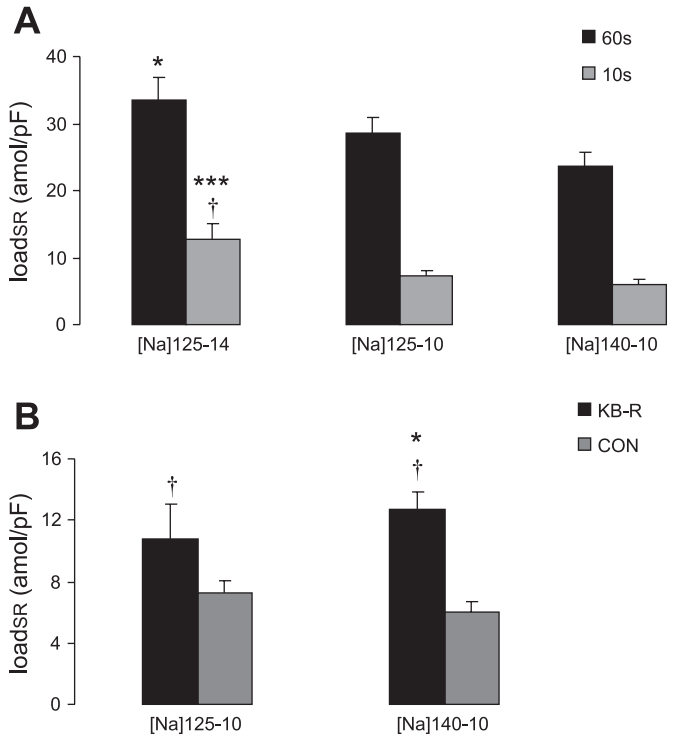

Fig. 6. $Load_{SR}$ (normalized by E_m) was affected by NCX activity in 3d myocytes. *A*: $load_{SR}$ in 10-s (gray bars) and 60-s (solid bars) intervals were determined using 3 different $[Na^+]_o/[Na^+]_i$ ratios (in mM): 125/14, 125/10, and 140/10. Significant differences were noted regarding $load_{SR}$ for 10-s interval between 125/14 and 125/10 mM and 140/10 mM (***$P < 0.005$ and †$P < 0.001$, respectively) and for the 60-s interval between 140/10 vs. 125/14 mM (*$P < 0.05$). No significant differences were observed regarding the 10-s interval between 125/10 and 140/10 mM or regarding the 60-s interval between 125/10 vs. 125/14 mM and 140/10 mM. $n = 15$. *B*: 10-s $load_{SR}$ was significantly increased in the presence of 30 μM KB-R (solid bars) in both 125/10 and 140/10 mM groups compared with control groups (gray bars). †$P < 0.001$. Magnitude of the increase was significantly greater in 140/10 than in 125/10 mM $[Na^+]_o/[Na^+]_i$ ratios. $n = 5$; *$P < 0.05$.

(see Supplemental Fig. 2). Therefore, although the data in this study clearly support SOCE in the regulation of $load_{SR}$, the evidence for a role of IP_3 in SOCE in cardiomyocytes is equivocal and requires further experimentation.

It has been reported that changes in intracellular $[Mg^{2+}]$ ($[Mg^{2+}]_i$) have an inhibitory effect on SOCE mediated by certain TRPCs (12, 38) by the binding of Mg^{2+} to the channel pore. However, extracellular $[Mg^{2+}]_o$ has not yet been shown to have an effect on SOCs. For example, Warnat et al. (39) found that a change of $[Mg^{2+}]_o$ from 0 to 2 mM had no effect SOCE in TRP4 channels expressed in Chinese hamster ovary (CHO) cells. In the present study, the substitution of $[Ca^{2+}]_o$ with $[Mg^{2+}]_o$ from 1 to 3 mM was consistently applied in all age groups for a short time (~10 s) to improve seal stability. Therefore, the transient increase of $[Mg^{2+}]_o$ is not likely to have an effect on the interpretation of our conclusions.

Role of NCX in SOCE in cardiac myocytes. Theoretically, the SOCE observed upon readdition of Ca^{2+} after exposure to Ca^{2+}-free extracellular solution could result from reverse mode NCX if the NCX reversal potential (E_{NCX}) at 2 mM $[Ca^{2+}]_o$ and 150 nM $[Ca^{2+}]_i$ in 3d myocytes (17) becomes more negative than −80 mV. This in turn would require that the subsarcolemmal $[Na^+]$ ($[Na^+]_s$) exceed 18 mM during prolonged perfusion with 0 mM $[Ca^{2+}]_o$ (see Supplemental Table 1). We used two different approaches to limit $[Na^+]_s$ accumulation. First, SR Ca^{2+} depletion was achieved by perfusing the cell with 25 μM CPA, 10 μM Ry, and 2 mM $[Ca^{2+}]_o$ instead of pretreatment with 0 mM $[Ca^{2+}]_o$, because the time needed to reach SR Ca^{2+} depletion in this manner may result in $[Na^+]_s > 18$ mM. Second, a 10-s perfusion time of 0 mM $[Ca^{2+}]_o$ (Figs. 3 and 5) resulted in a change of $[Ca^{2+}]_i$ that was <10% of the observed $[Ca^{2+}]_i$ after switching to 2 mM $[Ca^{2+}]_o$. We submit, therefore, that the $[Ca^{2+}]_i$ rise after switching $[Ca^{2+}]_o$ from 0 to 2 mM in the present study was a consequence of SOCE only (Figs. 3 and 5).

In addition, $load_{SR}$ was $[Na^+]_o$ and $[Na^+]_i$ dependent (Fig. 6*A*), which is explained by the resultant changes in E_{NCX} (estimated to be −40, −50 and −77 mV for 140/10, 125/10, and 125/14 mV combinations, respectively; see Supplemental Table 1), and this dependence was abolished by 30 μM KB-R (Fig. 6*B*). One might argue that this slight modification of $[Na^+]_o$ and $[Na^+]_i$ might have an effect on either the Na^+/K^+ pump or Na^+/H^+ exchanger (NHE), which could have altered intracellular Ca^{2+} homeostasis in our experiments. However, experiments performed at the laboratories of Bers and Vaughn-Jones (4, 41) showed that variations in $[Na^+]_i$ from 7 to 16 mm have little or no effect on NHE. Furthermore, both $load_{SR}$ (Fig. 2*A*) and elevation of $[Ca^{2+}]_i$ (Fig. 3*A*) under resting conditions were not blocked by 5 μM KB-R, a dose that effectively inhibited reverse mode NCX (see Supplemental Fig. 3), but instead were significantly increased in the presence of 30 μM KB-R, a dose reported to inhibit both reverse and forward mode NCX (1, 40) (Figs. 4 and 5, *B* and *C*), with the caveat that 30 μM KB-R is a relatively high dose. Therefore, this evidence strongly supports the notion that forward mode NCX efficiently competes with the SR Ca^{2+} pump for Ca^{2+} entering through SOC and agrees with a study by Chernaya et al. (9), who used transfected CHO cells that expressed bovine cardiac NCX. The present study was conducted at room temperature to preserve myocyte function and to prevent potential temperature gradients created by the rapid application of various solutions. This nonphysiological temperature results in an attenuation of both sarco(endo)plasmic reticulum Ca^{2+}-ATPase (SERCA) and NCX activities. However, we think that our conclusions would remain qualitatively the same, although there might be quantitative differences, if the experiments had been conducted at physiological temperatures (37°C).

However, such a predominant role of forward mode NCX in limiting SOCE-dependent $load_{SR}$ is contrary to observations in smooth muscle, neuronal, and nonexcitable cells, in which SR/ER Ca^{2+} refilling occurs primarily by reverse mode NCX activity (24). The reasons for this difference are not clear but may be related to different underlying mechanisms of SOCE. In particular, the selectivity of Ca^{2+} over Na^+ and the fact that the activity of NCX in cardiac myocytes is more than 10-fold greater than that in smooth muscle (35), combined with the much slower kinetics of smooth muscle contraction, could critically alter the role of NCX in SOCE-dependent SR refilling.

Voltage dependence of SOCE. Assuming that the contribution of the sarcolemmal Ca^{2+} pump is minimal, the magnitude of $load_{SR}$ appears to depend on competition between the SR Ca^{2+} pump and forward mode NCX for the SOCE. Thus more negative voltages increase the driving force for both SOCE (Fig. 5*B*) and forward mode NCX (Fig. 7). At a holding

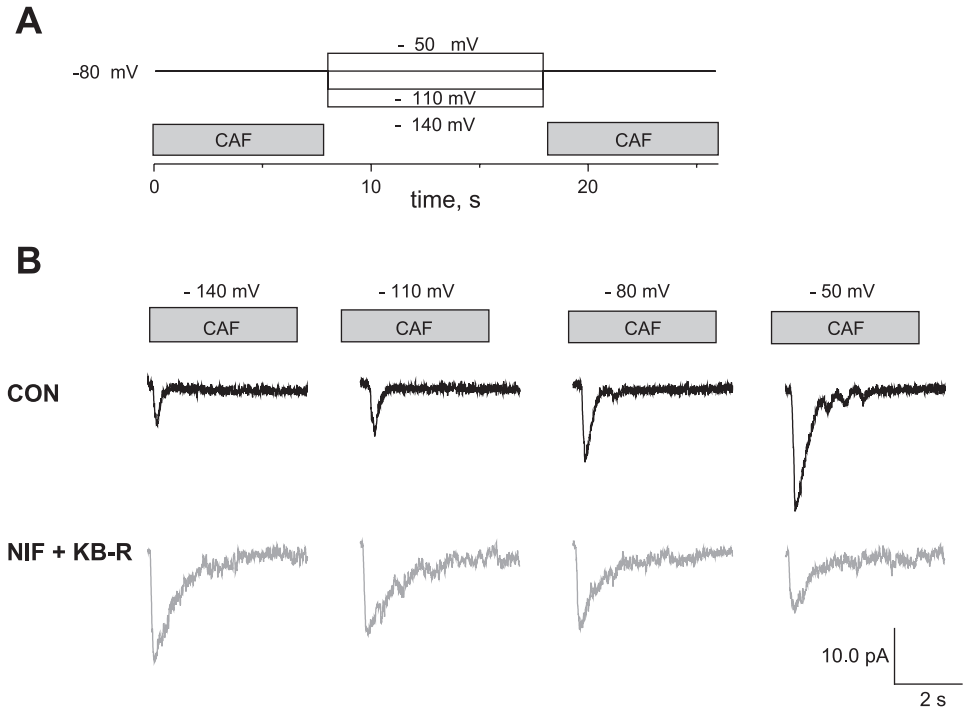

Fig. 7. Voltage dependence of $load_{SR}$ in 3d myocytes. *A*: protocol used for determination of voltage dependence of $load_{SR}$. The integral of I_{NCX} induced by the second CAF application was used to calculate $load_{SR}$. *B*: representative membrane traces induced by second CAF, with CON, and with 10 μM NIF plus 30 μM KB-R (NIF + KB-R). *C*: $load_{SR}$ (normalized by E_m) as a function of voltage in both CON (black traces) and NIF + KB-R (gray traces). There were significant increases in $load_{SR}$ by less negative membrane potentials (E_m). $^{**}P < 0.005$ and $^{*}P < 0.05$ for −80 mV vs. −50 mV and −80 mV vs. −110 mV, respectively. Conversely, there were significant decreases in $load_{SR}$ induced by less negative E_m in the presence of NIF + KB-R. $\dagger P < 0.05$. Slope of regression line (dashed gray line) was -0.20 amol·pF^{-1}·mV^{-1}. $n = 8$.

potential of −50 mV, the greater $load_{SR}$ appears to be the consequence of Ca^{2+} entry by reverse mode NCX and/or L-type I_{Ca}, because it is dramatically reduced by the presence of 10 μM NIF and 5 μM KB-R. $Load_{SR}$ exhibited linear voltage dependence on E_m in the presence of 30 μM KB-R, consistent with an increased driving force for SOCE at more negative E_m values and with the fact that SOCs are not voltage-gated channels. Therefore, $load_{SR}$ in the presence of 30 μM KB-R is more likely to reflect the actual SOCE, which is about twofold greater than that observed without KB-R.

Developmental changes in SOCE. Both the rise in $[Ca^{2+}]_i$ when $[Ca^{2+}]_o$ was switched from 0 to 2 mM (Fig. 3) and the $load_{SR}$ observed during resting conditions (Fig. 1) were significantly greater in 3d than in 56d myocytes, even though the 60-s $load_{SR}$ was only ~50% of the steady-state $load_{SR}$ in 3d myocytes (61.9 amol/pF) (17). In the present study, $load_{SR}$ after the 10-s interval was ~10 and 2 amol/pF in 3d and 56d myocytes, respectively, producing average SOC currents of 0.2 and 0.04 pA/pF, respectively, assuming that SOC exhibits high Ca^{2+} selectivity that is too small to be detected using the whole cell voltage patch-clamp technique. These values are considerably lower than the SOC density of ~0.7 pA/pF at −90 mV in rat cardiomyocytes reported recently by Hunton and colleagues (19, 20). It should be taken into consideration that SOC density of 0.7 pA/pF is similar to the peak I_{NCX} density elicited by 10 mM CAF in the rat and that it would load the adult rat SR at rest within 20–30 s. This suggests that the reported SOC density of 0.7 pA/pF is likely overestimated, possibly because of prolonged exposure to Ca^{2+}-free extracellular solution and the use of Ca^{2+} chelators and ionophores. Furthermore, the likelihood of higher surface-to-volume ratios in the younger age groups could yield appreciable $[Ca^{2+}]_i$ changes as well as the underestimation of $load_{SR}$ normalized by cell membrane surface (pF) (14). Therefore, although the increased $[Ca^{2+}]_i$

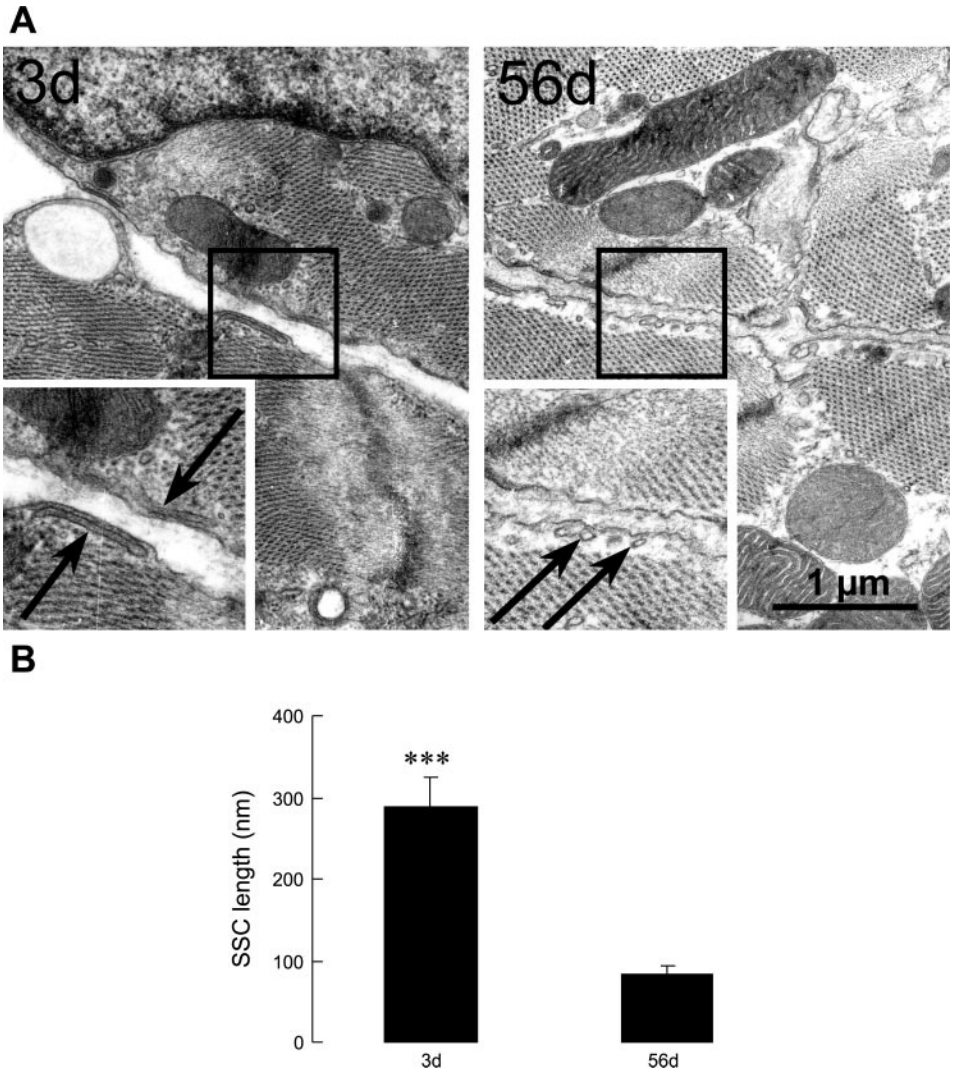

Fig. 8. Cross-sectional electron photomicrographs of subsarcolemmal cisternae (SSCs) from 3d and 56d ventricular tissue. *A*: representative cross-sectional images showing 3d and 56d myocytes. Scale bar, 1 μm; *insets*: SSCs shown at greater (×1.67) magnification. Abundant sheetlike and tubular SSCs (arrows) were observed in the 3d and 56d myocytes, respectively. Cleft between sarcolemma (SL) and SR is ~20 nm for both 3d and 56d myocytes. *B*: bar graph showing average SSC length, which was significantly greater (~3-fold) in 3d than in 56d myocytes. $n = 3$ hearts; 25 sections from each heart were used for analysis. $***P < 0.001$.

(Fig. 3) might be overestimated, it would not change the conclusion of developmental change in SOCE due to the strong support from the developmental change in $load_{SR}$.

Close spatial relationships between SOC, NCX, and SERCA2A within a microdomain are unique to neonatal myocytes. In the absence of SR Ca^{2+} pump inhibition during the 60-s period of $load_{SR}$ (Figs. 1*B* and 2*A*), there was no detectable increase in Ca^{2+} fluorescence (Fig. 3). Therefore, it is likely that Ca^{2+} influx into a microdomain between the sarcolemma and the SR through the SOCs is pumped back to the SR by SERCA before it reaches the bulk phase cytosol (29). As predicted, blockade of SERCA with CPA revealed SOCE as a rise in $[Ca^{2+}]_i$. The efficiency of transfer of Ca^{2+} from SOCE to SERCA depends on the spatial relationship between SERCA and SOC and the kinetics of SR Ca^{2+} uptake and SOCE. SOCE has an overall lower rate compared with SR Ca^{2+} uptake rate (11), presumably as a consequence of their relative densities (15). Thus little or no increase in $[Ca^{2+}]_i$ would be expected if SOCs were in proximity to the SR Ca^{2+} pump. Page and Buecker (28) found that before the development of a T-system (~10 days after birth), the surface density of dyads as well as total dyad areas per unit of cell volume and per unit of myofibrillar volume increase progressively during embryogenesis until they approach constancy at near-adult rabbit values 1 day after birth. Furthermore, in the present study, we have presented the novel finding of the abundant sheetlike SSCs in 3d myocytes in contrast to tubular SSCs in 56d myocytes. This finding, as well as the narrow cleft (20 nm) between SL and SR (Fig. 8), provides strong structural support for the existence of a distinct SL microdomain and thus the functional link between SOC, SERCA2A, and NCX in neonatal cardiomyocytes. The functional studies conducted at our and other laboratories have shown that there is a much greater SR Ca^{2+} content than previously recognized and that reverse mode NCX plays a more important role in excitation-contraction (E-C) coupling in the early developmental stages (17, 18). Furthermore, we have demonstrated a significantly greater time delay between the peaks of I_{NCX} and Ca^{2+} transient induced by rapid CAF application in myocytes from the youngest age groups (287 ms in 3d vs. 64 ms in 20d), as well as a significantly greater amount of Ca^{2+} already pumped out at the time of peak Ca^{2+} transient (50% of total Ca^{2+} in 3d vs. 17% of total Ca^{2+} in 20d) (17). These results support the hypothesis that there are ultrastructural differences in the subsarcolemma SR microdomain (17, 34) as a function of ontogeny. We propose, therefore, that NCX, SOC, and SERCA are in prox-

imity to each other in the 3d myocyte as reported with regard to mature smooth muscle (27). We postulate that the depletion of SR Ca^{2+} in neonatal ventricular myocytes triggers SOCs, which brings Ca^{2+} into a restricted microdomain between the SL and peripheral SR membrane in the neonatal heart. Because NCX has a substantive impact on SOCE-dependent $load_{SR}$, it must be close enough to the SOC to be able to compete effectively with SERCA for SOCE. In addition, both NCX and SERCA might contribute to normal heart function by preventing an increase in $[Ca^{2+}]_i$ during SR Ca^{2+} refilling. Further examination of the proximity of the proteins proposed in this model is required.

Mechanism and function of SOCE. Because it has commonly been accepted that SOCE does not exist in cardiomyocytes, the mechanism and function of SOCE in heart was not investigated until Hunton et al. (19) suggested that SOC might be involved in Ca^{2+}-mediated hypertrophy in rat cardiomyocytes. The present study is the first report of developmental regulation of SOCE, and these findings may be consistent with the observations of the latter study in that this period of ontogeny is characterized by substantial cardiomyocyte hypertrophic growth. In our study, myocyte surface area increased by >470% during the 3d–56d period on the basis of measurement of membrane capacitance (14.2 ± 0.5 vs. 68.0 ± 0.9 pF, respectively).

As a result of the apparently low unitary conductance and density of SOC, SOCE is unlikely to make a significant contribution to E-C coupling even in the neonatal myocyte. Thus the SOCE-dependent $load_{SR}$ of ~10 amol·pF^{-1}·10 s^{-1} in the 3d myocyte corresponds to an uptake rate of 6.4 μM/s (assuming a conversion factor of 6.44 pF/pl), which is ~10% of the total Ca^{2+} transient. However, the data suggest that SOCE is likely to play an important role in maintaining SR Ca^{2+} homeostasis, especially in the neonatal heart.

In conclusion, our results show that in the newborn rabbit, there is a robust reloading of SR Ca^{2+} (after CAF-induced clearance of SR Ca^{2+} content) mediated by SOCE and strongly modulated by NCX activity, suggesting that SOC, SERCA2A, and NCX are colocalized within a subsarcolemmal microdomain. Although the SOCE-dependent $load_{SR}$ is estimated to be too slow to contribute significantly to cytosolic Ca^{2+} cycling on a beat-to-beat basis, SOCE-dependent $load_{SR}$, together with NCX, may play an important role in SR Ca^{2+} homeostasis in the neonatal heart. This orchestrated interplay between SOCE, NCX, and SERCA2A may be of particular importance during open heart surgery in the neonate, in which an alteration of this balance could lead to uncontrolled SOCE-dependent $load_{SR}$ and arrhythmogenesis.

GRANTS

The generous support of the Canadian Institutes of Health Research and the Heart and Stroke Foundation of British Columbia and Yukon (to G. F. Tibbits) is gratefully acknowledged. J. Huang is the recipient of a Canada Research Scholarship from the Canadian Institutes of Health Research. L. Hove-Madsen is the recipient of a "Ramon y Cajal" grant from the Spanish Ministry of Science and Technology, and G. F. Tibbits is the recipient of a Tier I Canada Research Chair.

REFERENCES

1. **Amran MS, Homma N, and Hashimoto K.** Pharmacology of KB-R7943: a Na^+-Ca^{2+} exchange inhibitor. *Cardiovasc Drug Rev* 21: 255–276, 2003.
2. **Barritt GJ.** Receptor-activated Ca^{2+} inflow in animal cells: a variety of pathways tailored to meet different intracellular Ca^{2+} signalling requirements. *Biochem J* 337: 153–169, 1999.
3. **Berridge MJ.** Calcium oscillations. *J Biol Chem* 265: 9583–9586, 1990.
4. **Bers DM, Barry WH, and Despa S.** Intracellular Na^+ regulation in cardiac myocytes. *Cardiovasc Res* 57: 897–912, 2003.
5. **Biln P, Lin E, Huang J, Sedarat F, Moore ED, and Tibbits G.** Na^+-Ca^{2+} exchanger (NCX) in ventricular neonate myocytes is not homogenously distributed on the sarcolemma (SL) (Abstract). *Biophys J* 86: 554A, 2004.
6. **Braun FJ, Aziz O, and Putney JW Jr.** 2-Aminoethoxydiphenyl borate activates a novel calcium-permeable cation channel. *Mol Pharmacol* 63: 1304–1311, 2003.
7. **Casteels R and Droogmans G.** Exchange characteristics of the noradrenaline-sensitive calcium store in vascular smooth muscle cells or rabbit ear artery. *J Physiol* 317: 263–279, 1981.
8. **Cauvin C and van Breemen C.** Effects of Ca^{2+} antagonists on isolated rabbit mesenteric resistance vessels as compared with rabbit aorta. In: *Cardiovascular Effects of Dihydropyridine-Type Calcium Antagonists and Agonists*, edited by Fleckenstein A, van Breemen C, Gross R, and Hoffmeister F. Berlin, Germany: Springer-Verlag, 1985, p. 259–269.
9. **Chernaya G, Vázquez M, and Reeves JP.** Sodium-calcium exchange and store-dependent calcium influx in transfected Chinese hamster ovary cells expressing the bovine cardiac sodium-calcium exchanger: acceleration of exchange activity in thapsigargin-treated cells. *J Biol Chem* 271: 5378–5385, 1996.
10. **Fasolato C, Hoth M, Matthews G, and Penner R.** Ca^{2+} and Mn^{2+} influx through receptor-mediated activation of nonspecific cation channels in mast cells. *Proc Natl Acad Sci USA* 90: 3068–3072, 1993.
11. **Freichel M, Schweig U, Stauffenberger S, Freise D, Schorb W, and Flockerzi V.** Store-operated cation channels in the heart and cells of the cardiovascular system. *Cell Physiol Biochem* 9: 270–283, 1999.
12. **Hermosura MC, Monteilh-Zoller MK, Scharenberg AM, Penner R, and Fleig A.** Dissociation of the store-operated calcium current I_{CRAC} and the Mg-nucleotide-regulated metal ion current MagNuM. *J Physiol* 539: 445–458, 2002.
13. **Herrera AM, Kuo KH, and Seow CY.** Influence of calcium on myosin thick filament formation in intact airway smooth muscle. *Am J Physiol Cell Physiol* 282: C310–C316, 2002.
14. **Hoerter J, Mazet F, and Vassort G.** Perinatal growth of the rabbit cardiac cell: possible implications for the mechanism of relaxation. *J Mol Cell Cardiol* 13: 725–740, 1981.
15. **Hove-Madsen L and Bers DM.** Sarcoplasmic reticulum Ca^{2+} uptake and thapsigargin sensitivity in permeabilized rabbit and rat ventricular myocytes. *Circ Res* 73: 820–828, 1993.
16. **Hu HZ, Gu Q, Wang C, Colton CK, Tang J, Kinoshita-Kawada M, Lee LY, Wood JD, and Zhu MX.** 2-Aminoethoxydiphenyl borate is a common activator of TRPV1, TRPV2, and TRPV3. *J Biol Chem* 279: 35741–35748, 2004.
17. **Huang J, Hove-Madsen L, and Tibbits GF.** Na^+/Ca^{2+} exchange activity in neonatal rabbit ventricular myocytes. *Am J Physiol Cell Physiol* 288: C195–C203, 2005.
18. **Huang J, Xu L, Thomas MJ, Whitaker K, Hove-Madsen L, and Tibbits GF.** L-type Ca^{2+} channel function and expression in neonatal rabbit ventricular myocytes. *Am J Physiol Heart Circ Physiol* 290: H2267–H2276, 2006; doi:10.1152/ajpheart.01093.2005.
19. **Hunton DL, Lucchesi PA, Pang Y, Cheng X, Dell'Italia LJ, and Marchase RB.** Capacitative calcium entry contributes to nuclear factor of activated T-cells nuclear translocation and hypertrophy in cardiomyocytes. *J Biol Chem* 277: 14266–14273, 2002.
20. **Hunton DL, Zou L, Pang Y, and Marchase RB.** Adult rat cardiomyocytes exhibit capacitative calcium entry. *Am J Physiol Heart Circ Physiol* 286: H1124–H1132, 2004.
21. **Krautwurst D, Degtiar VE, Schultz G, and Hescheler J.** The isoquinoline derivative LOE 908 selectively blocks vasopressin-activated nonselective cation currents in A7r5 aortic smooth muscle cells. *Naunyn Schmiedebergs Arch Pharmacol* 349: 301–307, 1994.
22. **Kurebayashi N and Ogawa Y.** Depletion of Ca^{2+} in the sarcoplasmic reticulum stimulates Ca^{2+} entry into mouse skeletal muscle fibres. *J Physiol* 533: 185–199, 2001.
23. **Launikonis BS, Barnes M, and Stephenson DG.** Identification of the coupling between skeletal muscle store-operated Ca^{2+} entry and the inositol trisphosphate receptor. *Proc Natl Acad Sci USA* 100: 2941–2944, 2003.

24. **Lee CH, Poburko D, Sahota P, Sandhu J, Ruehlmann DO, and van Breemen C.** The mechanism of phenylephrine-mediated $[Ca^{2+}]_i$ oscillations underlying tonic contraction in the rabbit inferior vena cava. *J Physiol* 534: 641–650, 2001.
25. **Maruyama T, Kanaji T, Nakade S, Kanno T, and Mikoshiba K.** 2APB, 2-aminoethoxydiphenyl borate, a membrane-penetrable modulator of Ins $(1,4,5)P_3$-induced Ca^{2+} release. *J Biochem (Tokyo)* 122: 498–505, 1997.
26. **Merritt JE, Armstrong WP, Benham CD, Hallam TJ, Jacob R, Jaxa-Chamiec A, Leigh BK, McCarthy SA, Moores KE, and Rink TJ.** SK&F 96365, a novel inhibitor of receptor-mediated calcium entry. *Biochem J* 271: 515–522, 1990.
27. **Moore ED, Etter EF, Philipson KD, Carrington WA, Fogarty KE, Lifshitz LM, and Fay FS.** Coupling of the Na^+/Ca^{2+} exchanger, Na^+/K^+ pump and sarcoplasmic reticulum in smooth muscle. *Nature* 365: 657–660, 1993.
28. **Page E and Buecker JL.** Development of dyadic junctional complexes between sarcoplasmic reticulum and plasmalemma in rabbit left ventricular myocardial cells: morphometric analysis. *Circ Res* 48: 519–522, 1981.
29. **Poburko D, Kuo KH, Dai J, Lee CH, and van Breemen C.** Organellar junctions promote targeted Ca^{2+} signaling in smooth muscle: why two membranes are better than one. *Trends Pharmacol Sci* 25: 8–15, 2004.
30. **Poggioli J and Putney JW Jr.** Net calcium fluxes in rat parotid acinar cells: evidence for a hormone-sensitive calcium pool in or near the plasma membrane. *Pflügers Arch* 392: 239–243, 1982.
31. **Putney JW Jr.** The integration of receptor-regulated intracellular calcium release and calcium entry across the plasma membrane. *Curr Top Cell Regul* 31: 111–127, 1990.
32. **Putney JW Jr and Bird GS.** The inositol phosphate-calcium signaling system in nonexcitable cells. *Endocr Rev* 14: 610–631, 1993.
33. **Putney JW Jr, Broad LM, Braun FJ, Lièvremont JP, and Bird GS.** Mechanisms of capacitative calcium entry. *J Cell Sci* 114: 2223–2229, 2001.
34. **Sedarat F, Lin E, Moore ED, and Tibbits GF.** Deconvolution of confocal images of dihydropyridine and ryanodine receptors in developing cardiomyocytes. *J Appl Physiol* 97: 1098–1103, 2004.
35. **Slaughter RS, Shevell JL, Felix JP, Garcia ML, and Kaczorowski GJ.** High levels of sodium-calcium exchange in vascular smooth muscle sarcolemmal membrane vesicles. *Biochemistry* 28: 3995–4002, 1989.
36. **Trafford AW, Díaz ME, Negretti N, and Eisner DA.** Enhanced Ca^{2+} current and decreased Ca^{2+} efflux restore sarcoplasmic reticulum Ca^{2+} content after depletion. *Circ Res* 81: 477–484, 1997.
37. **Uehara A, Yasukochi M, Imanaga I, Nishi M, and Takeshima H.** Store-operated Ca^{2+} entry uncoupled with ryanodine receptor and junctional membrane complex in heart muscle cells. *Cell Calcium* 31: 89–96, 2002.
38. **Voets T, Prenen J, Fleig A, Vennekens R, Watanabe H, Hoenderop JGJ, Bindels RJM, Droogmans G, Penner R, and Nilius B.** CaT1 and the calcium release-activated calcium channel manifest distinct pore properties. *J Biol Chem* 276: 47767–47770, 2001.
39. **Warnat J, Philipp S, Zimmer S, Flockerzi V, and Cavalié A.** Phenotype of a recombinant store-operated channel: highly selective permeation of Ca^{2+}. *J Physiol* 518: 631–638, 1999.
40. **Watano T, Kimura J, Morita T, and Nakanishi H.** A novel antagonist, no. 7943, of the Na^+/Ca^{2+} exchange current in guinea-pig cardiac ventricular cells. *Br J Pharmacol* 119: 555–563, 1996.
41. **Wu ML and Vaughan-Jones RD.** Interaction between Na^+ and H^+ ions on Na^+-H^+ exchange in sheep cardiac Purkinje fibers. *J Mol Cell Cardiol* 29: 1131–1140, 1997.
42. **Zhang S, Yuan JXJ, Barrett KE, and Dong H.** Role of Na^+/Ca^{2+} exchange in regulating cytosolic Ca^{2+} in cultured human pulmonary artery smooth muscle cells. *Am J Physiol Cell Physiol* 288: C245–C252, 2005.